










The glacial geomorphology of the Río Corcovado, Río Huemul and Lago Palena/General Vintter valleys, northeastern Patagonia (43°S, 71°W)

Tancrède P. M. Leger ^a, Andrew S. Hein ^a, Robert G. Bingham ^a, Mateo A. Martini ^{b,c,d}, Rodrigo L. Soteres ^{b,c}, Esteban A. Sagredo ^{b,c,e} and Oscar A. Martínez ^f

^aSchool of GeoSciences, The University of Edinburgh, Edinburgh, UK; ^bMillenium Nucleus Paleoclimate, ANID Millenium Science Initiative, Santiago, Chile; ^cInstituto de Geografía, Facultad de Historia, Geografía y Ciencia Política, Pontificia Universidad Católica de Chile, Santiago, Chile; ^dCentro de Investigaciones en Ciencias de la Tierra (CICTERRA, CONICET-Facultad De Ciencias Exactas, Físicas y Naturales, UNC), Córdoba, Argentina; ^eEstación Patagonia de Investigaciones Interdisciplinarias UC, Pontificia, Universidad Católica de Chile, Santiago, Chile; ^fFacultad de Ciencias Naturales y Ciencias de la Salud, Universidad Nacional de la Patagonia San Juan Bosco, Esquel, Argentina

ABSTRACT

This study presents the first detailed glacial geomorphological map of the sediment-landform assemblages formed by three eastern outlet glaciers of the former Patagonian Ice Sheet. These glaciers occupied the Río Corcovado, Río Huemul and Lago Palena/General Vintter valleys, Chubut province, Argentina (43°S, 71°W). By combining remote sensing and field-mapping, we build on previous ice-sheet scale mapping and geological surveys to provide high-resolution spatial information on local ice-contact glaciogenic, glaciofluvial, glaciolacustrine, and subglacial landforms. Twenty-five landform types, many of which are newly mapped in the region, were digitized as georeferenced shapefiles over a 5300 km² area. This map enables the identification of former ice-flow directions, relative ice-margin positions and glaciofluvial drainage pathways for each preserved Quaternary glaciation. It also elucidates the former areal extent, geolocation and spillways of glaciolacustrine bodies formed during the last deglaciation. The map delivers an essential framework on which to build robust glacier-scale geomorphological and geochronological reconstructions.

ARTICLE HISTORY

Received 22 May 2020
Revised 9 July 2020
Accepted 9 July 2020

KEYWORDS




Patagonia; glacial geomorphology; Quaternary landscape evolution; Río Corcovado glacier; Río Huemul glacier; Lago Palena/General Vintter glacier


1. Introduction

The Patagonian region of southern South America was host to the most extensive Quaternary ice sheet of the southern hemisphere outside of Antarctica, the Patagonian Ice Sheet (PIS). The PIS covered a latitudinal extent of ~2000 km (38°S–56°S; Figure 1) along the spine of the Patagonian and Fuegian Andes (Caldenius, 1932; Davies et al., 2018, 2020; Glasser et al., 2008; Martínez et al., 2011). Patagonia is part of the only continental landmass that fully intersects the precipitation-bearing southern westerly winds (Garreaud et al., 2013) and is one of few regions in the southern mid-latitudes containing a well-developed Quaternary glacial geomorphological record (Clapperton, 1993; Glasser et al., 2008). Patagonia therefore offers a unique opportunity to study Quaternary climatic and environmental change in the southern mid-latitudes.

Robust palaeoglaciological reconstructions of PIS outlet glaciers can help us to investigate the landscape evolution and climate-forcing mechanisms responsible for Quaternary ice-sheet fluctuations (e.g. Hein et al., 2010; Rabassa et al., 2000). They can provide insights into the timing and causes of Quaternary glacial cycles

in the southern mid-latitudes, and enable determination of the regional drivers of glaciation as well as inter-hemispheric glacial (a)synchronicity (Bentley et al., 2005; Denton et al., 1999; Glasser et al., 2008). For these reasons, the PIS has been subject to an increasing number of glacial geochronological reconstructions. However, with a few exceptions (e.g. García et al., 2019; Iglesias et al., 2016; Van Daele et al., 2016) there remains a general lack of published detailed mapping and geochronological data across the northeastern sector of the former ice sheet, between ~39°S and ~46.5°S (Darvill et al., 2015; Davies et al., 2020; Mendelová et al., 2017). Robust reconstructions from this region are needed to understand fully the PIS response to the Last Glacial Maximum (LGM) at these latitudes, and to investigate latitudinal dependencies on the timing of the local LGM throughout Patagonia (Darvill et al., 2015; Davies et al., 2020; García et al., 2018; 2019; Sagredo et al., 2011). A vital component of such reconstructions is detailed, glacier-scale geomorphological mapping (Chandler et al., 2018; Clark et al., 2018; Evans & Orton, 2015). This provides spatial information that facilitates interpretations of

CONTACT Tancrède P. M. Leger  Tancrede.leger@ed.ac.uk  School of GeoSciences, The University of Edinburgh, Institute of Geography, Drummond Street, Edinburgh EH8 9XP, UK;  @https://twitter.com/legertancrede?lang=en

 Supplemental data for this article can be accessed <https://doi.org/10.1080/17445647.2020.1794990>.

© 2020 The Author(s). Published by Informa UK Limited, trading as Taylor & Francis Group on behalf of Journal of Maps

This is an Open Access article distributed under the terms of the Creative Commons Attribution License (<http://creativecommons.org/licenses/by/4.0/>), which permits unrestricted use, distribution, and reproduction in any medium, provided the original work is properly cited.

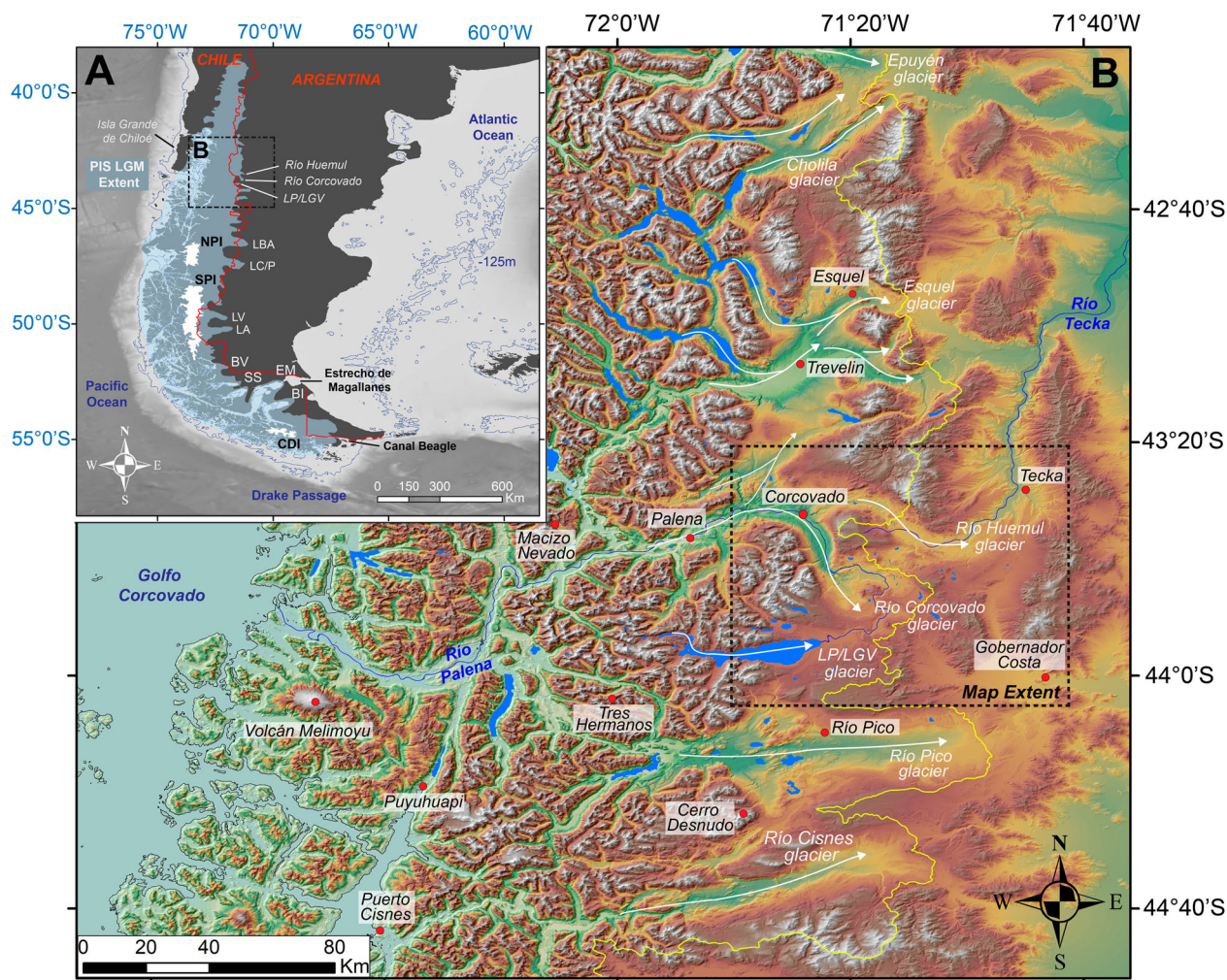


Figure 1. Geographical and glaciological context of the study area. (A) Approximate former extent of the Patagonian Ice Sheet (PIS) at the Last Glacial Maximum (LGM), redrawn after Glasser et al. (2008) and Glasser and Jansson (2008). Overlain in white are the contemporary North Patagonian (NPI), South Patagonian (SPI), and Cordillera Darwin (CDI) Icefields. Major eastern PIS glaciers are designated; BI: Bahía Inútil, EM: Estrecho de Magallanes, SS: Seno Skyring, BV: Bella Vista, LV: Lago Viedma, LC/P: Lago Cochrane/Pueyrredón, LBA: Lago Buenos Aires. Bathymetric data of ocean basins were obtained from the General Bathymetric Chart of the Oceans (GEBCO) and are displayed in greyscale. A -125 m contour line is applied to simulate the approximate former position of coastlines at the LGM (Lambeck et al., 2014). The Chile/Argentina border is highlighted in red. (B) Digital elevation model (DEM) of northern Patagonian region from the ALOS WORLD 3D missions (version 2.2; JAXA; <https://www.Eorc.jaxa.jp/ALOS/en/aw3d30/>) with a shaded relief background and a black sea level contour line highlighting modern coastlines. White arrows indicate former ice-flow of major northeastern PIS outlets, including the Río Corcovado, Río Huemul and Lago Palena/General Vintter glaciers. The yellow line designates the contemporary Atlantic/Pacific drainage divide. Lake bodies and key river channels are drawn in blue. The black dotted box delineates the extent of the geomorphological map presented with this paper.

palaeoglaciological behaviour and equips glacial geologists with an essential framework upon which to build robust chronologies (Chandler et al., 2018; Bendle et al., 2017a; Darvill et al., 2016). We thus present in this paper the first detailed glacial geomorphological map of three valleys in northeastern Patagonia (43.5°S), the Río Corcovado, Río Huemul and Lago Palena/General Vintter valleys (Figure 1b). Our aim is to provide benchmark geomorphological data for future geochronological interpretations of their glacial history.

2. Study location and previous work

The geomorphological map is centred on a region located east of the Patagonian Andes, between 43.3°S

and 44.0°S , and covers an area of ~ 5300 km² (Figure 1b). At these latitudes, a major westward-dipping over-deepened valley, the Río Palena trough, cuts through the Andes to drain the contemporary Río Corcovado, Río Huemul and Lago Palena/General Vintter catchments westward to the Pacific Ocean. At this location, the PIS was characterised by ice flowing towards the east-northeast from the centre of the former ice sheet, located near Macizo Nevado. Glacier ice thus flowed along the Río Palena trough to the mountain front, where it diverged into two glaciers occupying the Río Huemul valley to the east, and the Río Corcovado valley to the south (Figure 1b). The two outlet glaciers extended up to 60 km to the east and southeast of the Argentinian town of Corcovado

(43°54'S; 71°46'W) (Caldenius, 1932; Haller et al., 2003; Martínez et al., 2011). Here, we refer to these as the Río Huemul glacier and the Río Corcovado glacier; the latter to distinguish it from the Golfo Corcovado outlet glacier that drained the western side of the PIS (Denton et al., 1999). The Lago Palena/General Vintter outlet glacier drained a separate, smaller catchment located ~30 km southeast of the Río Palena trough. This glacier flowed eastward, at times extending to converge with the Río Corcovado glacier coming from the north (Figure 2). Subsequent retreat into an over-deepened basin led to the formation of the moraine-dammed Lago Palena/General Vintter lake, still present to this day (43°55'S; 71°31'W) (Figure 2). Our mapping focuses on the former terminal environment of these three outlet glaciers. Subglacial erosion and over-deepening of the Río Palena trough is greater towards the centre of the former PIS where ice thickness and duration of ice cover were largest (Clapperton, 1993; Hubbard et al., 2005; Kaplan et al., 2009). Thus, at our study site, asymmetrical subglacial erosion generated a progressive eastward migration of the Atlantic-Pacific drainage divide following each Quaternary glaciation, causing the contemporary drainage divide to be located ~70–80 km east of the central spine of the Andes (Davies et al., 2020; Kaplan et al.,

2009) (Figure 2). The semi-arid eastern sectors of the Río Corcovado, Río Huemul and Lago Palena/General Vintter valleys, which belong to the Patagonian steppe climate zone, are characterised by extensive, well-preserved and easily discernible moraine complexes, along with their associated glaciofluvial and glaciolacustrine sediment-landform assemblages (Haller et al., 2003; Martínez et al., 2011).

Geomorphological mapping of major moraine limits in the Río Corcovado, Río Huemul and Lago Palena/General Vintter valleys was conducted by Caldenius (1932), Glasser and Jansson (2008), and Davies et al. (2020), in their respective efforts to record the glacial geomorphology of the entire PIS (Table 1). Haller et al. (2003), meanwhile, produced a regionally-focused geological map of the three valleys including main glaciogenic deposits (area located between 43–44°S and 72–70.3°W). These deposits were also mentioned in studies by Lapido (1990) and Martínez (2002; Martínez et al., 2011). However, all previous mapping was part of ice-sheet-wide geomorphological investigations or geological surveys and was focused primarily on identifying the most prominent moraines and glaciofluvial deposits for each glaciated valley. All previous studies interpreted the landforms as Pleistocene glaciogenic deposits associated with three distinct glaciation

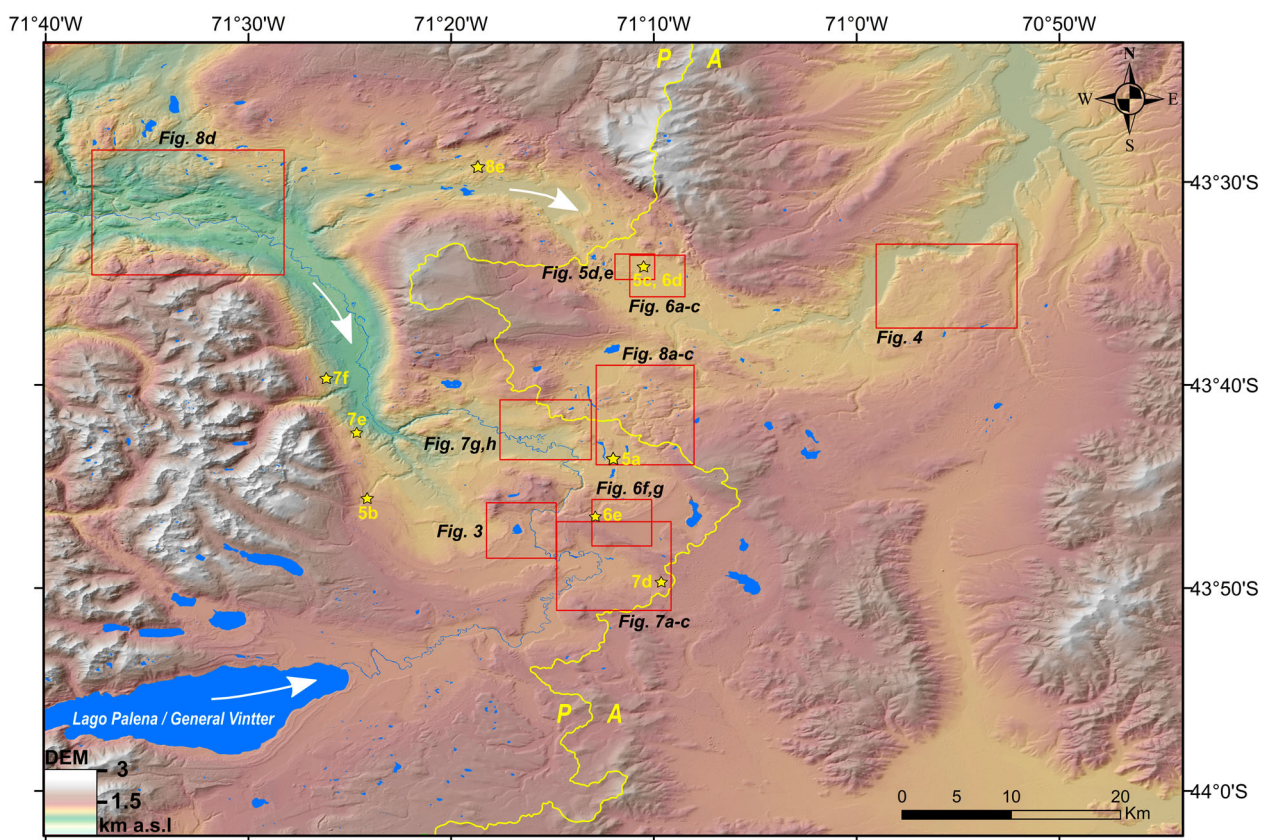


Figure 2. Digital elevation model (AW3D30 and hillshade) showing the area covered by the map presented with this paper. Locations of imagery / geomorphology comparison maps presented in Figures 3–8 are shown by red boxes. Locations of photographs presented in Figures 3–8 are indicated with yellow star symbols. The Atlantic (A) / Pacific (P) drainage divide is delineated in bright yellow, while ice-flow direction of the Lago Palena/General Vintter, Río Corcovado and Río Huemul glaciers is indicated by the white arrows. The Río Corcovado and lakes / water bodies are mapped in dark blue.

Table 1. Summary of mapped glacial landform morphologies, identification criteria from remote sensing, mapping uncertainties and previous mapping conducted in the Río Corcovado, Río Huemul and Lago Palena/General Vintter valleys.

Feature/ landform	Morphology	Identification criteria from remote sensing	Mapping uncertainties	Palaeoglaciological significance	Previous mapping
Moraine ridges	Distinct linear to arcuate shaped, steep-sided (20–40°) and continuous (>200 m) ridges displaying positive relief (5–45 m), a clear break-of-slope, and sharp undulating crests.	Easily identified on DEM hillshade if prominent enough as light-shadowing highlights positive relief with arcuate, narrow shape. Dark grey in colour on DG imagery. Different in texture to surrounding terrain (Figure 5d).	May be difficult to identify heavily subdued ridges from imagery for oldest ice marginal deposits. Lower relief moraine ridges can in some cases be confused with palaeo-shorelines.	Indicate former ice-front position. Prominence, crest undulation, continuity and slope gradients combined can be indicators of erosion and relative age of moraine deposit / glacial advance.	Glasser and Jansson (2008); Davies et al. (2020) (main features only)
Hummocks	Rounded to sub-rounded mounds of glaciogenic sediments arranged chaotically.	Best identified on high-resolution imagery although sometimes possible from DEM. Dark grey or brown in colour on Digital Globe (DG) imagery, although lighter than meltwater channels. Sub-rounded light shadowing demonstrates positive relief (Figure 4a).	May be challenging to identify limits of feature from remote sensing for relatively old, subdued deposits, or in vegetated areas.	Indicate marginal ice contact.	Unmapped
Hummocky ridges	Mounds of glaciogenic sediments arranged in a linear fashion and generating a distinct ridge crest of limited length (<300 m).	Best identified on high-resolution imagery although sometimes possible from DEM. Dark grey or brown in colour on DG imagery, although lighter than meltwater channels. Narrow, linear light shadowing demonstrates positive relief and ridge structure (Figure 3a)	May be challenging to map accurately for older deposits due to erosion and lack of prominence, thus creating potential for under-discovery. In such cases, differentiation between moraine and hummocky ridges can be less conspicuous. Although no eskers were explicitly identified in the area, some may have been mis-interpreted as hummocky ridges.	Indicate marginal ice contact. Abundant, prominent, and parallel ridges are likely to suggest substantial till deposition and thus a relatively stable, long-lasting glacier margin.	Unmapped
Moraine complexes	Relatively confined, narrow (<3 km) and easily discernible drift belts of arcuate shape comprising prominent and continuous moraines ridges as well as concentrated, parallel hummocky ridges.	Best identified on high-resolution imagery. Dark grey or brown in colour deposit belts composed of hummocks, hummocky and moraine ridges, and different in colour to surrounding terrain e.g. proglacial outwash plains (Figure 3a).	May be challenging to identify limits of feature for relatively old deposits, or vegetated areas.	Indicate former glacier front positions following glacial advance or still-stand.	Caldenius (1932); Haller et al. (2003); Glasser and Jansson (2008); Davies et al. (2020) (main features only)
Kettle holes	Circular to semi-circular / elongate hollows and pits of shallow depth (<20 m).	Best identified from high-resolution imagery. Light grey/white circular to elongate pockmarks, may be water-filled. No perceivable light-shadowing as no positive relief (Figure 4a).	Potential for under-discovery in areas exploited by subsequent and/or modern drainage. Depressions can also be exploited by modern lacustrine bodies and thus be confused with features characteristic of modern hydrology.	Indicates former presence of ice front. High feature concentration can mark presence of progressively thinning and stagnant ice.	Unmapped
Kettle-kame topography	Extensive (>3 km in width) drift deposits composed of chaotic and disorganised hummocks (or kames) irregularly interspersed with hollows and kettle holes.	Best identified from high-resolution imagery. Areas comprising high concentration of chaotically arranged kettle holes, small lakes, hummocks and hummocky ridges. Such glaciogenic deposits gives the ensemble a dark grey or brown colour on DG imagery (Figure 4a).	May in some cases be difficult to identify the boundary with moraine complexes as difference between an organised, arcuate group of glaciogenic sediment and a more scattered form of hummocky terrain can be open to doubt.	Indicates former ice-marginal zone, possibly under a stagnant, dead-ice front scenario.	Unmapped
Proglacial outwash plains	Broad, low-gradient surfaces composed of fluviially-rounded sand- and gravel-sized sediment, in some cases prograding from former ice-margins. Can demonstrate former braided meltwater channel networks on their surfaces.	Feature limits identified from imagery, although broad terrace characteristics make it distinguishable from DEM. Little to no positive relief, light brown to orange in colour, and imagery can reveal surface channels. Feature limits often associated with fluvial incision scarps (Figure 6a,f).	Surface grading can be difficult to distinguish from remote sensing (DEM only) and it can be challenging to identify the limits of outwash features from imagery.	Indicates former pathways of meltwater during glacier advance or still-stand.	Caldenius (1932); Glasser and Jansson (2008); Davies et al. (2020) (main features only)
Meltwater channels	Incised sinuous conduits formed by larger discharge regimes than contemporary runoff, commonly occurring as highly concentrated	Dark brown sinuous conduits, discernible from high-resolution imagery on proglacial outwash plains due to darker colour. Large	Potential for under-discovery when former drainage pathways are re-exploited by modern runoff. Braided channel systems can	Indicates former detailed pathways and flow-direction of glacial metlwater. Their	Unmapped

(Continued)

Table 1. Continued.

Feature/ landform	Morphology	Identification criteria from remote sensing	Mapping uncertainties	Palaeoglaciological significance	Previous mapping
	multi-channel systems with in many cases no association with modern drainage.	(>30 m) isolated channels can display light-shadowing due to negative relief (e.g. Figure 6a,f).	be challenging to distinguish from imagery on older outwash plain deposits.	abundance and ease of discovery can be a good proxy for age of glaciofluvial deposit.	
Fluvial incision scarps	Continuous break-in-slope with relatively steep surface gradients (20–40°), curving basal convexities and sharp concave crests.	Discernible from DEM in cases of significant incision (>20 m) due to break in slope, but also from imagery in vegetation-free areas, due to sudden colour and/or texture change between features and light shadowing due to steep incision slope (e.g. Figure 5e,d)	Can be mis-interpreted and/or difficult to identify from remote sensing when fluvial incision is not sufficient to appear on DEM (<20–30 m). Possible confusion (although unlikely) with landslide/rockslide or tectonic scarps.	Marks location and patterns of fluvial incision into deposits. If located across outwash plains, they mark different regimes of meltwater flux and sediment loading, which can sometimes serve as a proxy for glacial advances / still-stands.	Unmapped
Possible GLOF deposits	Fan-shaped, sub-aerial deposit prograding from the mouth of a tributary valley and demonstrating fluvial sorting, but displaying large (b axis >1 m) imbricated boulders and braided surface channels wider than modern runoff allows. Such features can also be associated with large breaches in terminal moraines damming nested lakes.	Characteristics and sedimentology of unique feature identified as such were discussed on the field. (see paragraph 4.3.4.). Smooth terrace characteristics and post-deposition incision of feature are discernible from DEM. Fan shape and wide surface channels can be distinguished from imagery.	Although mapped separately, the one deposit mapped as such requires a more specific and detailed geomorphological and sedimentological investigation to produce a more confident interpretation. There is potential for mis-interpretation here.	Indicate former high-magnitude, sudden flood event mobilising substantial quantities of till material.	Unmapped
Palaeo-shorelines	Very linear, continuous, undulating and smooth outline of sediment, characterised by a mono elevation-interaction with topography. Sometimes easy to discern from imagery when numerous, parallel ridges can be observed following contour lines over tens of kilometres.	Only visible from high-resolution imagery due to lack of positive relief. Appear as gently curving lines spread across slopes at single elevations and alternating in colour between light and dark brown (in vegetation-free areas), particularly discernible when numerous shorelines run parallel to each other (Figure 7a).	If one isolated, discontinuous feature is identified, there is potential for confusion with a low-relief moraine ridge or other linear features such as an esker (although not so likely).	Mark former lake surface level. In the case of an ice-dammed lacustrine system, it can also indicate the lowest elevation of a usable drainage spillway.	Unmapped
Raised deltas	Fan-shaped feature of fluvially deposited sands and gravel, deposited near tributary valley mouths, with similar properties to alluvial fans. However a raised delta is nested on modern valley slopes and unused by modern hydrology (often incised post-depositionally). It's prograding slope does not reach the valley floor: but instead an elevation matching observed palaeoshorelines, in some cases.	Can be identified from DEM due to homogeneous and smooth surface prograding towards valley floors and further incised by modern river channel. Fan-shaped and often lighter and different in texture than surrounding terrain. For vegetation-free cases, braided surface palaeochannels typical of alluvial fans can be distinguished.	Although features mapped as such were checked to match elevation of mapped and field-verified palaeo-shorelines, there is possibility of confusion (although unlikely) with ice-dammed proglacial outwash deposits from tributary glacier meltwater. If sedimentology wasn't verified on the field: such alluvial deposits could also be related to former GLOF deposits occurring during proglacial lake residence.	Can further designate former lake level.	Unmapped
Glaciolacustrine deposits	Deposit accumulations are characterised by distinctive white and light grey colouration on imagery. Easily eroded due to unconsolidated fine nature of sediments leading to distinct incision patterns and sharp crests.	Best visible in flat basins from imagery due to lack of positive relief. However DEM can reveal deeply incised exposures forming steep gorges through dark/light shadowing. Light grey to white in colour on DG imagery, their texture is distinct from surrounding terrain. (Figure 7g).	True extent of the sediment accumulations is easily underestimated from imagery. Field investigation is required to reduce such uncertainty.	Demonstrates existence and extent of former proglacial lake system.	Unmapped
Glacial lineations	Highly linear, parallel and relatively narrow landforms with length-to-width ratios of approximately 10:1 and aligned to former interpreted ice flow.	Visible either on DEM and hillshade for prominent features (>20 m) as positive relief generates dark/light shadowing, or on high-resolution imagery. Such linear, narrow and	Potential bias in former ice-flow interpretation can lead to mis-interpretations of a particular bedrock outcrop orientation as subglacially streamlined when outcrop orientation is	Marks former areas of relatively thick, fast-flowing and warm-based ice and indicates directionality of former ice-flow. Streamlining can be depositional (in the case of sediment	Glasser and Jansson (2008) ; Davies et al. (2020) (main features only)

(Continued)

Table 1. Continued.

Feature/ landform	Morphology	Identification criteria from remote sensing	Mapping uncertainties	Palaeoglaciological significance	Previous mapping
		elongated landforms often occur in groups of parallel features (Figure 8a,b).	instead related to tectonics, geological structural properties, slope failures or other geomorphic processes.	flutes for instance) or erosional (in the case of streamlined bedrock).	
Drumlinoid forms	Depositional linear hills characterised by oval to ellipsoidal shapes, significant positive relief (>10 m), and which are aligned to former interpreted ice flow.	Visible either on DEM (if prominent enough) or imagery. Features appear dark grey to brown in colour and display dark/light shadowing due to significant positive relief. They are non-undulating (linear) and oval/ellipsoidal in shape (Figure 4).	May be challenging to identify limits of feature for relatively old deposits (pre-LGM) and can be confused with sediment flutes (lineations). Identification bias due to former ice-flow knowledge is possible.	Marks former areas of relatively thick, fast flowing ice on low-gradient glaciogenic sediment surfaces.	Unmapped
Ice-moulded bedrock	Prominent bedrock outcrops ranging from 20 m to 1 km in width, displaying significant positive relief (>30 m) and located in areas of warm-based ice-flow (with high concentrations of lineations).	Large outcrops visible from DEM due to significant positive relief. Steep side-walls generate light shadowing on imagery. The light-to-dark grey and sometimes brown colour of exposed surfaces is often different than adjacent terrain, especially in more vegetated areas. Exposed surfaces display an irregular, rough texture (Figure 8d).	Possible confusion of small features with human infrastructure, although very unlikely given remoteness of field site.	Marks former areas of relatively thick, fast-flowing and warm-based ice causing efficient subglacial erosion. Large scale striations and plucking patterns can indicate former ice-flow directionality.	Unmapped
Contemporary channels / creeks	Any river channel used by modern runoff and detectable from remote sensing.	Large channels causing substantial incision can be discerned from DEM, however in vegetation-free areas high-resolution imagery enables clear identification of active or seasonally active channels and creeks.	Small creeks (<10 m width) sometimes surrounded or covered by vegetated terrain can be challenging to accurately locate from imagery. Mapping in such cases relies on computed watershed analysis using DEM data.	In recently (Quaternary) glaciated landscapes, the geometry of modern channels can demonstrate anomalies such as diversions from quickest downvalley path highlighting damming effect of glacial deposits on topography, thus aiding identification of ice margins.	Haller et al. (2003); Glasser and Jansson (2008 - Rio Corcovado only)
Atlantic-Pacific drainage divide	Line separating Atlantic versus Pacific- directed drainage of surface runoff. This line was generated by extrapolating drainage catchments from the AW3D30 DEM using a standard watershed analysis in ArcGIS.	Computed using DEM (AW3D30).	Geolocation uncertainties associated with DEM accuracy. Tarolli and Mudd (2019) report 90% linear errors to vary between 5 and 10 metres with a positive correlation to slope gradients for this dataset.	Current position of drainage divide indicates the effect and magnitude of subglacial erosion and valley over-deepening during cycles of Quaternary glaciations. It can also inform on the potential location of Atlantic-ward spillways of former ice-dammed lake systems following ice retreat into overdeepened basins.	Unmapped
Boglands	Accumulation of surface water and thus vegetation in areas of low surface gradients.	Appear as light to dark green areas composed of numerous small creeks / channels and/or small lakes, they are characterised by little to no positive relief (e.g. Figure 3).	When relying on imagery, natural bogland formation can be sometimes confused with anthropogenic irrigation of fields and agricultural practice.	Extensive bogland surfaces in arid steppe landscape can sometimes indicate former lacustrine and/or fluvial sediment deposition: as vegetation favours fine sediments. Can also indicate patterns of former meltwater pathways exploited by modern hydrology.	Unmapped
Rotational slump and landslides	Bowl-shaped area of a slope demonstrating a depression with steep upper break in slope (crown scarp), highlighting the exposed part of the steeper failure surface, and numerous parallel (transverse) scarps or fissures accumulated below.	Large features can be distinguished from DEM due to steep upper break in slope displaying dark/light shadowing. Transverse failure fissures and ridges located below the crown scarp are best identified on high-resolution imagery.	Possible confusion with large rock-slope failures in heavily vegetated zones. Transverse ridges or fissures enabling identification of slump can be confused with moraine or hummocky ridges, thus requiring field verification.	Demonstrates slope instability and large-scale mass wasting event; common in former paraglacial environments due to combination of glacial debuitting and atmospheric exposure of unconsolidated, unsorted and non-vegetated sediments.	Unmapped
Empty cirques	Bowl-shaped depression near mountain ridge tops with a concave floor open on its downhill side, and a steeper: cupped headwall on its uphill side	Can be distinguished from DEM due to steep headwall on many portions of bowl-shaped valley generating significant dark/light shading as well as sharp mountain ridges on cirque's boundaries.	Glacial cirques can, in some cases, be mistaken for bowl-shaped structural bedrock formations, thus not formed by glacier build-up and subglacial erosion.	Records local cirque glaciation during phases of ice-sheet advance/retreat.	Glasser and Jansson (2008) (features were re-mapped at higher spatial resolution)

events, with the innermost preserved moraines suggested to relate to the local LGM. However, the ages of Río Corcovado, Río Huemul and Lago Palena/General Vintter deposits were inferred solely from morpho-stratigraphic observations and comparisons with other dated Patagonian records (e.g. the Lago Buenos Aires record, 46.5°S), with numerical dating yet to be applied. Here, we thus undertake the first detailed mapping of the complex glacial sediment-landform assemblages preserved in the three valleys. This work will serve as a geomorphological framework for new geochronological reconstructions in progress.

3. Methods

3.1. Remote sensing

Initial identification of major landforms and topographic features was conducted using the ALOS WORLD 3D – 30 m resolution (AW3D30) Digital Elevation Model (DEM) (version 2.2; <https://www.Eorc.jaxa.jp/ALOS/en/aw3d30/>) (Figure 2). Hillshade backgrounds of different azimuths were produced using ArcGIS (v10.5), along with topographic contour lines. When displaying significant positive relief (>15 m), cross-section elevation profile graphs were generated to further distinguish major landforms according to their morphometry. All mapped landforms were digitised manually in the WGS84 geographic reference coordinate system using the ESRI™ World Imagery layer, characterised by 1.0 m resolution images from DigitalGlobe (GeoEye, IKONOS, 2000–2011) at the study site. To increase landform identification potential, three-dimensional views of this imagery layer were produced in the ‘Windows Maps’ application (Microsoft Corporation). In areas with high vegetation cover, different colour-rendering comparisons were made using 10 m resolution Sentinel 2A true colour (TCI) and false colour (bands 8,4,3) products (<https://scihub.copernicus.eu/>). Similar mapping methodologies were used by Martin et al. (2019), Darvill et al. (2014), Bendle et al. (2017a), Mendelová et al. (2020) and Soteres et al. (2020) to conduct high spatial resolution glacial geomorphological mapping of other Patagonian regions.

3.2. Field mapping

Field mapping was conducted over the austral summers of 2018 (Lago Palena/General Vintter only), 2019 and 2020 (all three valleys). Fieldwork focussed primarily on ground-truthing and/or corrections of preliminary landform interpretations, with additional geomorphological mapping undertaken in key accessible locations (Chandler et al., 2018). To aid understanding of landform genesis, landform sedimentology was also analysed where possible.

4. Results

4.1. Glacial geomorphology

The glacial geomorphology in the study area records the terminus positions of the Río Corcovado, Río Huemul and Lago Palena/General Vintter outlet glaciers over multiple glacial cycles. Glacial depositional and erosional features thus heavily dominate the three valleys’ geomorphological records. Our mapping reveals twenty-five landform types, classified and manually digitised as polyline and polygon shapefiles (Table 1). These comprise seventeen glacial geomorphological landform types, including a variety of ice-contact glaciogenic landforms (e.g. moraines, hummocks), glaciofluvial (e.g. outwash plains, meltwater channels), glaciolacustrine landforms (e.g. palaeo-shorelines, raised deltas) and sub-glacial landforms (e.g. ice-moulded bedrock, lineations). Identification criteria for these seventeen landforms are described below, and uncertainty assessments related to landform identification are summarised in Table 1. The map also features six geomorphological features providing wider geographical context, including empty cirques, alluvial fans, rotational slumps or landslides, and modern hydrological features (e.g. rivers, lakes etc.). Furthermore, a polyline delineates the contemporary Atlantic-Pacific drainage divide, extrapolated from the DEM (Figure 2).

4.2. Ice-contact glaciogenic landforms

4.2.1. Moraine complexes and kettle-kame topography

We differentiate here between two types of ice-contact glaciogenic sediment composites. Relatively confined, narrow (<3 km wide) and easily discernible sediment complexes of arcuate shape comprising prominent and continuous moraine ridges (Section 4.2.2), as well as concentrated, hummocky ridges in parallel to each other (Section 4.2.3), are here termed moraine complexes (Figure 3). In contrast, large (>3 km) deposits composed of chaotic hummocks (or kames) irregularly interspersed with hollows and kettle holes, presenting few moraine ridges and low concentrations of hummocky ridges, are here defined as kettle-kame topography (Darvill et al., 2014; Figure 4). Although both composites essentially highlight former glacier margins, we feel that it is important to distinguish between their dissimilar morphologies to highlight possible variability in former ice-marginal environments (e.g. Benn & Clapperton, 2000; Darvill et al., 2014; Raedeke, 1978). In contrast to well-defined moraine complexes diagnostic of the less extensive, younger deposits (Figure 3), the most distal deposits discernible from imagery and in the field in the Río Huemul valley consist of a large belt of kettle-kame topography, previously termed the ‘Tecka drift’ (Haller et al., 2003; Lapido, 1990; Martínez et al., 2011) (Figure 4). Consequently, differentiating

between distinct glaciogenic sediment compounds morphologies in our mapping can prove useful when producing subsequent geomorphological interpretations of local palaeoglaciological behaviour (Darvill et al., 2014).

4.2.2. Moraine ridges

The eastern sector of the mapped area exhibits numerous well-preserved landforms identified as linear- to arcuate-shaped, steep-sided (20° – 40°) ridges displaying positive relief (5–45 m), a clear break-of-slope, and sharp undulating crests. Such features were interpreted as moraine ridges (Benn & Evans, 2014) delineating former lateral and terminal ice-front margins; the moraine crests were mapped as polylines. Moraine ridges in the field can occur as well-preserved, cross-valley continuous ridges outlining former latero-terminal ice margins over several kilometres (Figure 5). However, they can also occur as fragmented, discontinuous and shorter ridges (a few hundred metres in length), clustered alongside multiple, smaller hummocky features. Well-preserved, prominent and continuous moraine ridges can be discerned from the DEM due to their significant positive relief and arcuate shape (Figure 2). Such moraine ridges are characteristic of the innermost moraine sequences of the Río Corcovado, Río Huemul and Lago Palena/General Vintter valleys, which are likely associated with the local LGM (Lapido, 1990; Martínez et al., 2011; Figure 5a,c). The older, more distal moraine complexes are morphologically distinct and characterised by wider, more subdued and broad-crested ridges. They also display lower slope gradients, making them more challenging to distinguish and map from imagery. In such older environments,

identifying ice limits can be problematic, and often requires the adjacent detection of other proglacial deposits such as kettle holes, meltwater channels and proglacial outwash plains, which on the Argentine forelands tend to remain better preserved than moraine ridges due to lower erosion and mass-wasting potential (Dunai, 2010; Hein et al., 2009, 2011). Thus, fewer prominent, continuous moraine ridges could be mapped for the older, most extensive moraine complexes of the study site.

4.2.3. Hummocks and hummocky ridges

Throughout the three valleys mapped in this study, we find an abundance of rounded to sub-rounded mounds of glaciogenic sediments, often termed hummocks in glacial geomorphology (Benn & Evans, 2014). When hummocks are arranged in short (<300 m wide) ridges of limited relief (<30 m), they are often described as hummocky ridges/moraines (Darvill et al., 2014; Eyles et al., 1999). Hummocky ridges were mapped as polylines along identified crestlines while distinct hummocks were mapped as polygons. These features are widespread throughout our study site and occur as; (1) isolated features in kettle-kame topography, where their linearity often originates from supraglacial or ice-contact glaciofluvial deposition (Darvill et al., 2014), or (2) ridges observed in latero-terminal moraine complexes, clustered in parallel successions orientated perpendicular to ice flow, sometimes alongside prominent moraine ridges (Figure 5e). In this latter case, hummocky ridges are likely to represent discontinuous recessional moraines, eroded and diminished by meltwater runoff

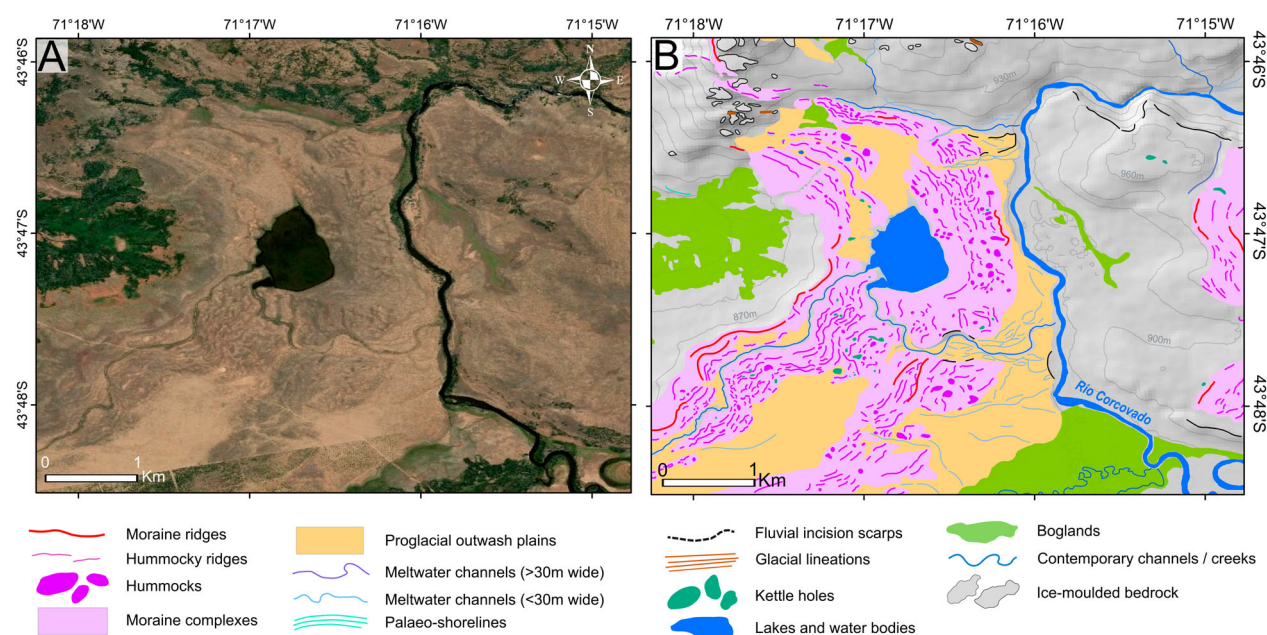


Figure 3. (A) Satellite imagery (ESRITM, DigitalGlobe) and (B) glacial geomorphological mapping comparison (contour lines interval: 30 m) of two-closely-spaced, well-defined terminal moraine complexes located in the Río Corcovado valley, to the east and south-east of the Arroyo El Fango headwaters. Despite being closely-spaced, the two moraine complexes are separated in most parts by a distinct proglacial outwash plain deposit which suggests that the innermost moraine complex represents a younger re-advance or still-stand of the Río Corcovado outlet glacier. See Figure 2 for location.

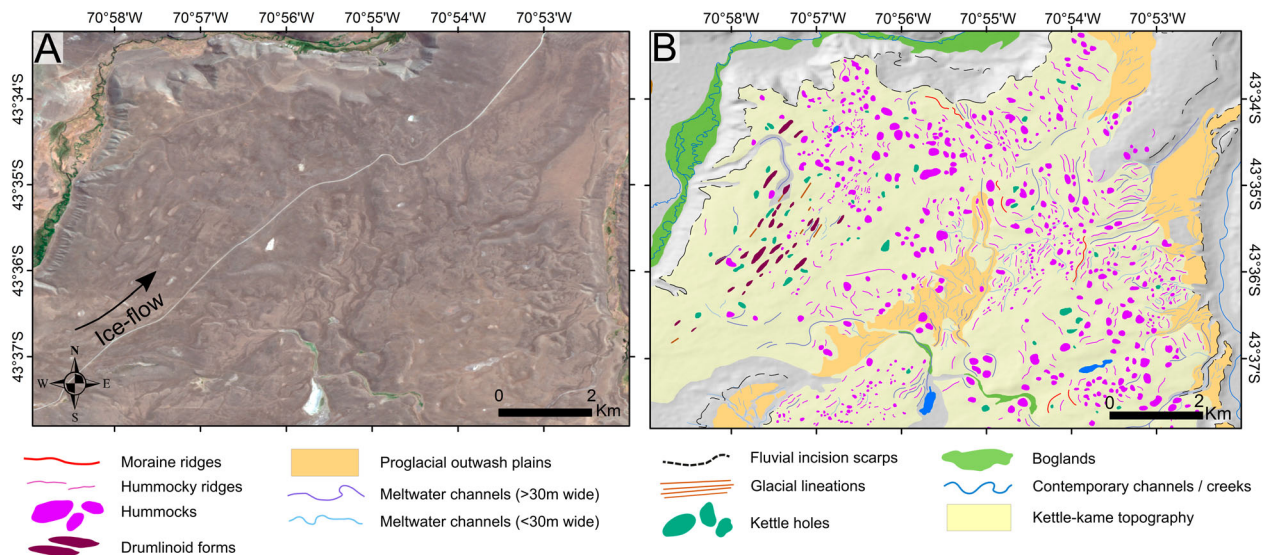


Figure 4. (A) Satellite imagery (Sentinel 2A TCI image 02/03 2018) and (B) glacial geomorphological mapping comparison of the Tecka Drift (as termed by Haller et al., 2003; Lapido, 1990; and Martínez et al., 2011) located to the east of the Río Huemul valley. This deposit is characterised, unlike moraine complexes, by a chaotic and extensive array of ice-contact glaciogenic mounds such as hummocks and hummocky ridges with low parallelism, interspersed with numerous kettle-holes and large (>30 m wide) former meltwater channels. Such a low-gradient deposit is diagnostic of a stagnant, progressively thinning ice front (dead-ice scenario), and was here mapped as kettle-kame topography. See Figure 2 for location.

(Clapperton et al., 1995; Eyles et al., 1999). On the other hand; abundant, highly concentrated, parallel- and perpendicular-to-ice-flow hummocky ridges can indicate a relatively stable ice margin, such as observed within the well-defined younger terminal moraine complexes located in the Río Corcovado valley, to the southeast of the Arroyo El Fango headwaters (Figure 3a,b).

4.2.4. Kettle holes

In both moraine complexes and kettle-kame topography of the Río Corcovado, Río Huemul and Lago Palena/General Vintter valleys, numerous examples of circular to semi-circular hollows and dry pits of shallow depth (<20 m) can be observed chaotically dispersed within hummocky terrain. We interpreted these features as kettle holes, which are landforms commonly associated with slowly retreating or stagnant glacier fronts (Evans & Orton, 2015; Price, 1969; Russell et al., 2006). Kettle holes are typically formed through burial of ice blocks by till and glaciofluvial sediments, leading to the formation of enclosed rounded depressions near the ice-margin as the ice block subsequently melts (Benn et al., 2007; Knight, 2011). Figure 4 depicts a complex of kettle holes distributed across kettle-kame topography within the southeastern latero-terminal margin of the former Río Huemul glacier (43°40'S; 70°55'W).

4.3. Glaciofluvial landforms

4.3.1. Proglacial outwash plains

Glaciofluvial outwash plains are characterised by broad, low-gradient surfaces composed of fluvially-rounded sands and gravels (Alloway et al., 2018; Darvill

et al., 2015; Denton et al., 1999; Evans & Orton, 2015; Hein et al., 2009). They often occur adjacent and down-valley to latero-frontal moraine systems and are sometimes associated with the presence of palaeo-meltwater channels (Coronato et al., 2013; Darvill et al., 2014). In the Río Corcovado, Río Huemul and Lago Palena/General Vintter valleys, numerous well-preserved outwash plains prograde on the ice-distal sides of moraine complexes and kettle-kame belts, with average slopes of $\sim 0.5^\circ$ – 1° (Figure 6). The younger outwash plains are often characterised by well-preserved former meltwater channels with clear braiding patterns (Figure 6c,g), while these features are less common for older deposits. At the older margins, the flat nature of outwash plains combined with the arid, windy conditions of the Argentine foreland often enables better preservation levels than their associated moraines (Bentley et al., 2005; Darvill et al., 2015; Hein et al., 2009, 2011, 2017; Smedley et al., 2016). Such long-term preservation properties make identifying outwash surfaces a vital component of mapping older ice-marginal environments.

4.3.2. Meltwater channels

Abandoned sinuous channels associated with former ice margins, and formed by larger discharge regimes than contemporary runoff would enable, are common across the glaciofluvial and glaciogenic depositional environments of the Río Corcovado, Río Huemul and Lago Palena/General Vintter valleys (Figure 6a,c,f,g). They were interpreted as former glacial meltwater channels, and commonly occur as concentrated multi-channel systems, braided and etched into the

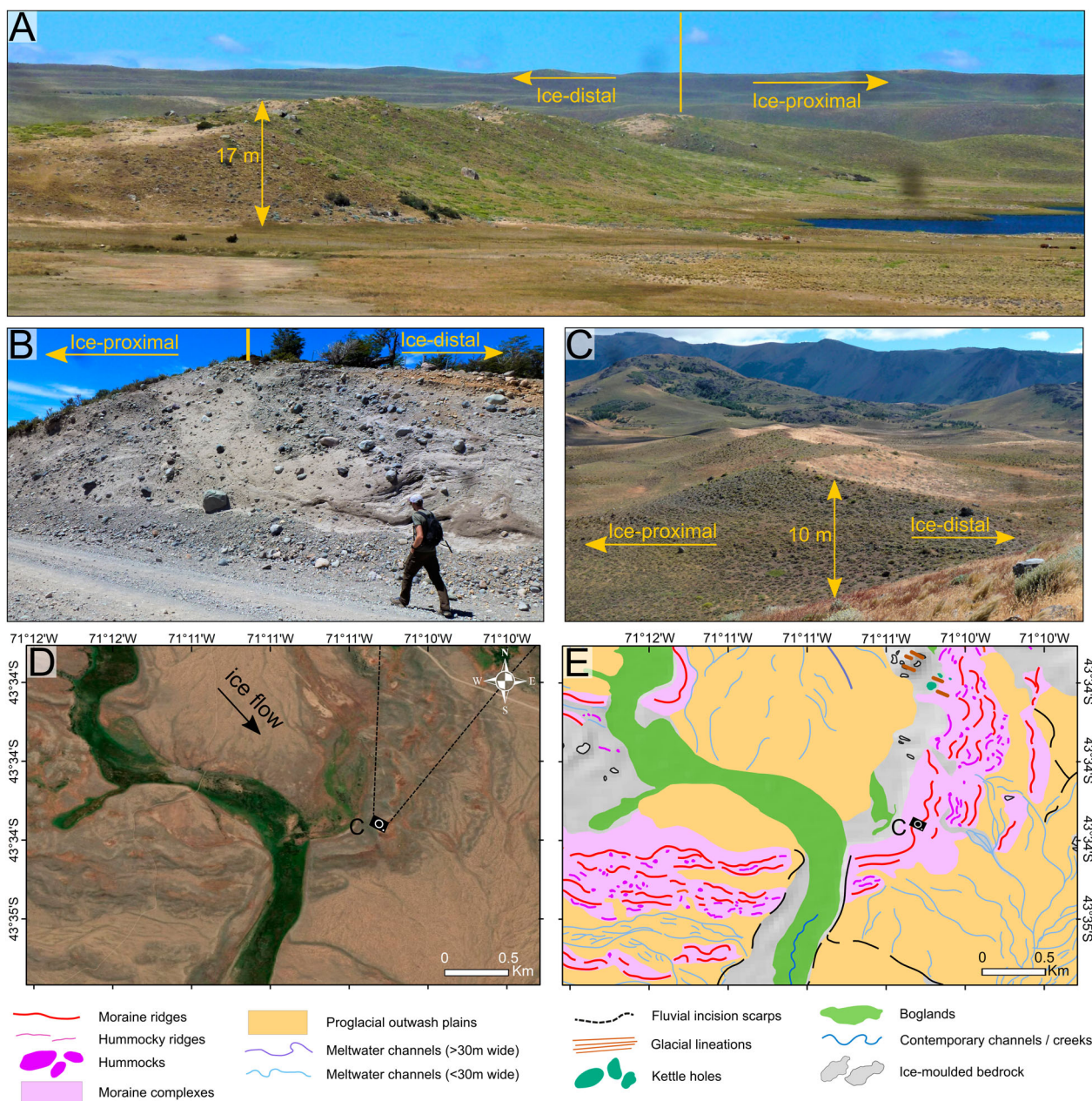


Figure 5. (A) View towards the south/southeast of a well-preserved, prominent terminal moraine in the eastern Río Corcovado basin (camera location: $43^{\circ}43'40.64''\text{S}$, $71^{\circ}12'2.48''\text{W}$). (B) Photograph of a road-cut section through a well-preserved latero-terminal moraine ridge of the Río Corcovado palaeoglacier western margin displaying glacio-tectonic till structures (location: $43^{\circ}45'37.99''\text{S}$, $71^{\circ}24'9.06''\text{W}$). (C) View towards the northeast as indicated on panel D (camera symbol) of a well-preserved terminal moraine ridge in the Río Huemul valley. (D) Satellite imagery (ESRITM, DigitalGlobe) and (E) glacial geomorphological mapping comparison of the well-preserved terminal moraine ridges located in the Río Huemul valley forming a well-defined arcuate moraine complex. Panels (D) and (E) also display two extensive proglacial outwash plains to the southeast (time-synchronous with photographed moraine – panel (D)) and the northwest (younger than photographed moraine) and exhibiting braided former meltwater channels. See Figure 2 for location.

surface of glaciofluvial outwash plains, with up to 5–10 m relief. Individual traceable channels vary in length between 100 m and 5 km and between 5 and 250 m in width. In low-gradient, lateral ice-marginal environments, wider palaeo channels (>30 m) can be found isolated within moraine complexes and oriented parallel to lateral moraine ridges and former ice flow. Such channels are abundant within the Río Huemul glacier's latero-terminal kettle-kame topography (Haller et al., 2003; Lapido, 1990; Martínez et al., 2011) (Figure 5).

In many instances across the field site, such large meltwater channels now act as natural pathways for contemporary, lower discharge drainage systems.

4.3.3. Fluvial incision scarps

Incision scarps are characterised by relatively steep surface gradients (20° – 40°), curving basal concavities and sharp convex crests and are locally formed by former or active river incision into till or glaciofluvial terrace deposits. These landforms were mapped as polylines

highlighting their upper breaks in slope. The location, concentration and preservation of incision scarps can prove useful when assessing changes in glacial and post-glacial fluvial discharge and sediment-load regimes. Identifying such features and their distribution can help to understand the incision and erosion patterns of former glaciogenic deposits and thus help to elucidate the lack of preserved glacial sediment-landform assemblages at a given location (Hein et al., 2017). Mapping such features can also facilitate the interpretation of former shifts in proglacial meltwater drainage pathways associated with different glacier front positions (Bentley et al., 2005). Furthermore, mapped scarps constitute useful data for fluvial geomorphologists wishing to investigate former terrace aggradations as indicators of former runoff regimes, sediment loads and local postglacial isostatic response (Mor-eiras et al., 2017; Olszak, 2011).

4.3.4. Glacial lake outburst flood deposits

At 43°33'S; 71°29'W, 2 km to the southwest of Corcovado, a unique deposit covering an area of ~2 km² was investigated. The landform is a fan-shaped, subaerial deposit prograding from the mouth of a tributary valley to the valley floor of the Río Corcovado valley. Its valley-floor elevation suggests it was deposited after the drainage of the proglacial lake occupying the valley. It is associated with a 500 m-wide breach through lineated subglacial deposits of the Río Corcovado glacier and has been incised into by the narrow (<10 m width) modern tributary river. A road-cut section of the 5 m thick deposit exhibits some evidence of fluvial sediment sorting. However, the deposit comprises a high concentration of large (b axis >1 m) rounded to sub-rounded imbricated boulders of varied lithologies, and exhibits wide (up to 25 m) braided surface channels discernible from imagery. Such characteristics are diagnostic of a sudden, high-magnitude mass-wasting event causing mobilisation of substantial till volumes (Blair, 2002; Russell et al., 2006). The landform was thus interpreted and mapped as a potential glacial lake outburst flood deposit. One possible source of floodwaters could have been waters dammed by ice or glacial deposits at the tributary head, now an empty cirque occupied by a 1200 m² lake (43°36'2"S; 71°33'2"W). Although this deposit requires further geomorphological and sedimentological investigation to produce a confident interpretation, we believe it is pertinent here to distinguish it from other alluvial deposits.

4.4. Glaciolacustrine landforms

4.4.1. Glaciolacustrine deposits

Numerous examples of extensive laminated glaciolacustrine sediment outcrops were found in the Río Corcovado and Río Huemul valleys along road and river cuttings, particularly in areas located on the ice-proximal side of the innermost moraine complexes, at elevations below 790 m (Figure 7). The glaciolacustrine

sediments are characterised by fine, occasionally laminated deposits of clay and silts (cf. Evans, 2014; Henríquez et al., 2017; Rabassa et al., 2000; Thorndycraft et al., 2019) (Figure 7e). On imagery, large sediment accumulations can appear as white and grey-coloured assemblages of heavily incised, fragmentary landforms (Figure 7g). Indeed, soft and unconsolidated glaciolacustrine deposits are more susceptible to post-depositional erosion than coarser till deposits and other proglacial sediment assemblages (e.g. glaciofluvial sands and gravels), especially in the semi-arid Argentine foreland (Bendle et al., 2017b; Thorndycraft et al., 2019). Such deposits indicate the former presence of substantial proglacial lake bodies following glacier recession. To decrease the potential for misinterpretation, we exclusively mapped glaciolacustrine deposits within flat basins enclosed by conspicuous palaeo-shorelines (Figure 7c,h).

4.4.2. Palaeo-shorelines

Platforms demonstrating a gently curving and convex frontal break of slope nested at single elevations and stretching over extensive distances (sometimes tens of kilometres) were interpreted as former notched proglacial lake shorelines (Glasser & Jansson, 2008; Hein et al., 2010; Sissons, 1978) (Figure 7d,f). Such erosional features can be discriminated from continuous moraine ridges through a lack of positive relief, a lower degree of sinuosity, and their occurrence at continuous elevations over great distances. Moreover, lake level fluctuations often lead to several palaeo-shorelines running parallel to each other and to topographic contour lines, which were used additionally to aid feature identification (Figure 7a,c). Well-preserved examples of palaeo-shorelines can be observed on the windier eastern slopes of the Río Corcovado valley, at elevations of 680 and 790 m (Figure 7f), as well as towards the terminal environment of the former Río Corcovado glacier, nested between 910 and 990 m in elevation (Figure 7a,c).

4.4.3. Raised deltas

The mapped region features several fan-shaped, smooth terrace surfaces gently sloping towards valley floors, yet nested distinctively above the valley floors. These deposits are composed of well-sorted, rounded sands and gravels indicating fluvial deposition near the mouths of tributary valleys. After matching the elevations of such features with abandoned palaeo-shorelines, we interpreted these terraces as raised lacustrine deltas formed by tributary rivers flowing into former proglacial lake systems (Bendle et al., 2017a, 2017b; Glasser et al., 2016). Raised deltas can serve as additional geomorphological evidence of former glaciolacustrine systems and help to identify their former surface elevations. For instance, a well-preserved raised delta can be discerned on the western flank of the Río Corcovado trough, perched on the southern edge of the

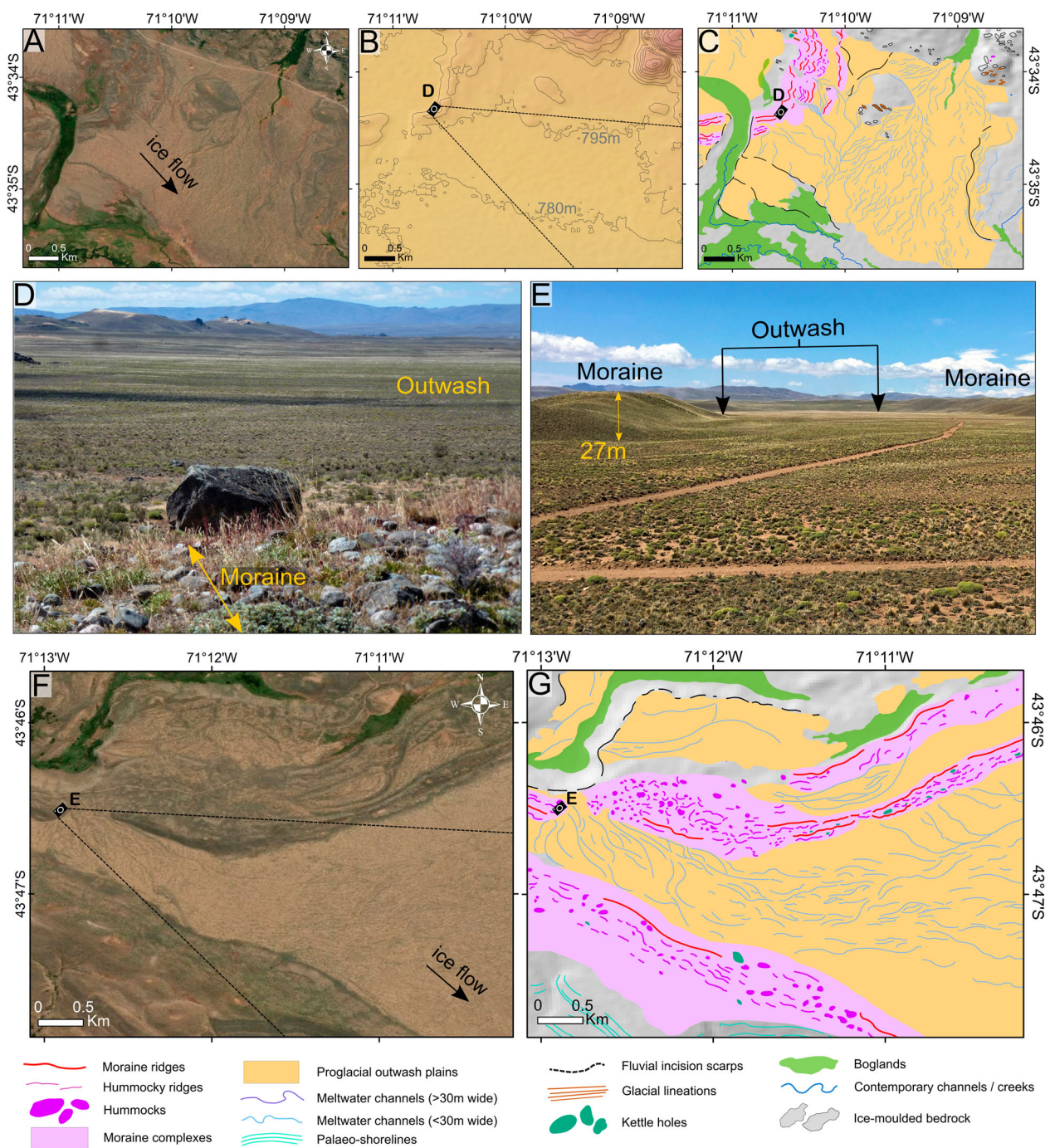


Figure 6. (A) Satellite imagery (ESRITM, DigitalGlobe), (B) DEM with topographic contour lines (15 m interval) and (C) glacial geomorphological mapping comparisons of an extensive, proglacial outwash plain of the Río Huemul valley, which exhibits remarkable preservation of now inactive braided meltwater channels. (D) View towards the Southeast (as shown on panel B) of the proglacial outwash plain formed when the Río Huemul glacier deposited the moraine ridge from which the photograph is taken (location: 43° 34'21.00''S, 71°10'32.82''W). (E) View towards the Southeast (as shown on panel F) of a well-preserved proglacial outwash plain confined between two prominent terminal moraine complexes of the Río Corcovado valley (location: 43°46'30.94''S, 71° 12'52.03''W). (F) Satellite imagery (ESRITM, DigitalGlobe) and (G) glacial geomorphological mapping comparisons of the proglacial outwash plain photographed (panel E), which demonstrate clear patterns of former braided meltwater channel systems. See Figure 2 for location.

Río Poncho Moro valley mouth (43°40'5''S; 71° 25'4''W). This landform sits at a similar elevation than the prominent 680 m palaeo-shoreline discerned within the valley. Large raised deltas like this specific example can be strong indicators of relatively stable proglacial lake systems (Bendle et al., 2017a; Hein et al., 2010; Turner et al., 2005).

4.5. Subglacial landforms

4.5.1. Glacial lineations, flutings, drumlinoid forms and ice-moulded bedrock

We identified linear, parallel and relatively narrow landforms displaying positive relief with length-to-width ratios of ~10:1 (Figure 8). Such features are

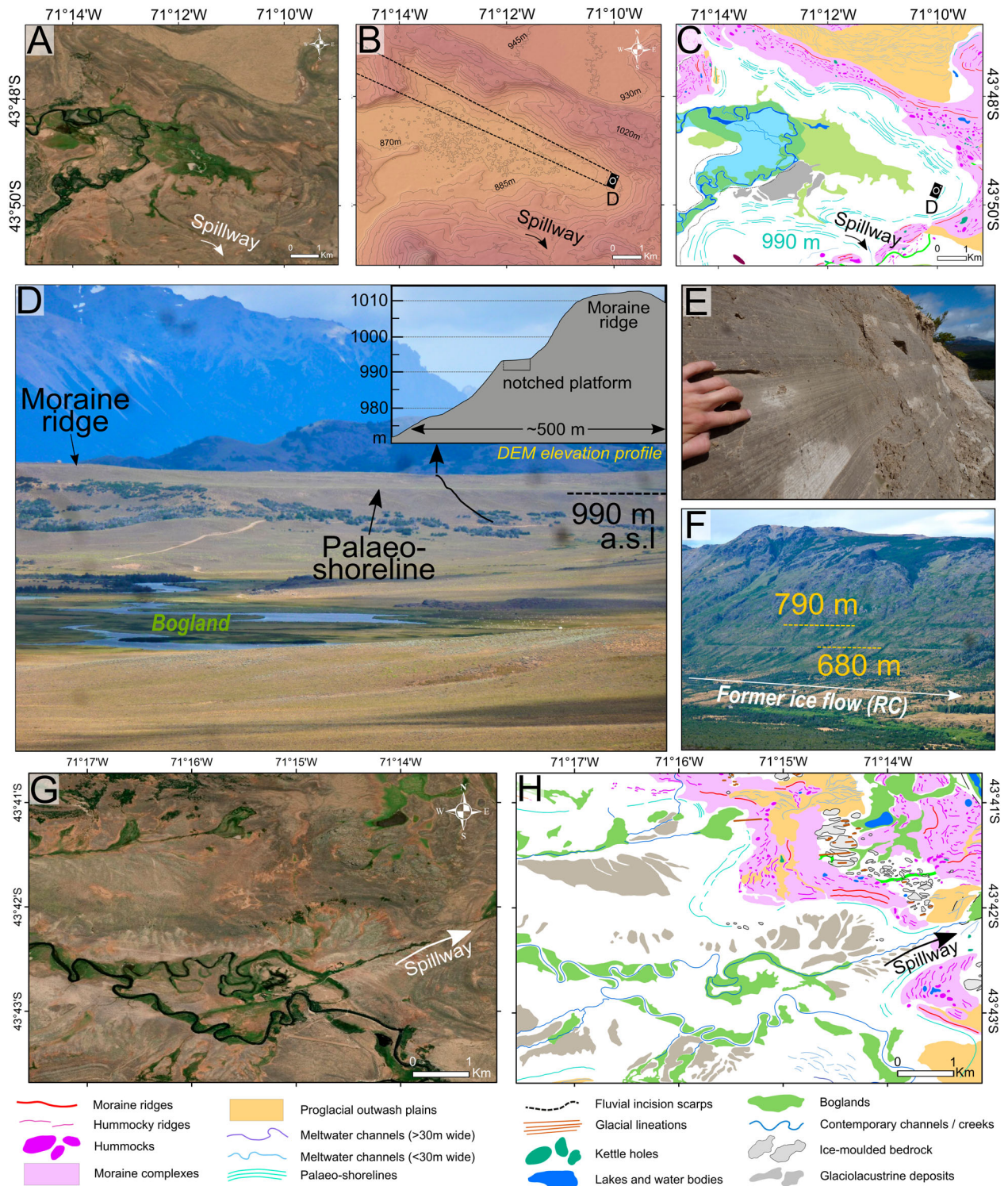


Figure 7. (A) Satellite imagery (ESRI™, DigitalGlobe), (B) DEM with topographic contour lines (15 m interval) and (C) glacial geomorphological mapping comparisons of a former glaciolacustrine basin in the Río Corcovado valley encircled by well-preserved, highly continuous and parallel palaeo-shorelines (nested between 910 and 990 m) running over tens of kilometres at singular elevations. The former lake basin floor displays a low gradient surface now host to the Río Corcovado as well as an extensive bogland. (D) View towards the northwest (as shown on panel B) of a palaeo-shoreline nested on the ice-distal slope of a terminal moraine ridge in the Río Corcovado valley. This shoreline is associated with the former proglacial lake, which resided in the basin mapped on panel C (camera location: 43°49'43.46''S, 71°9'54.92''W). An elevation profile graph extrapolated from DEM highlights the geomorphology of the palaeo-shoreline and adjacent moraine ridge. (E) Road cut section through well-preserved laminated varve sediments (location: 43°42'08,0''S, 71°24'41,6''W). (F) View towards the northeast of two continuous palaeo-shorelines cut into the eastern slopes of the Río Corcovado valley (camera location: 43°40'00,5''S, 71°26'26,0''W). (G) Satellite imagery (ESRI™, DigitalGlobe) and (H) glacial geomorphological mapping comparison of another, lower-elevation drained glaciolacustrine basin located in the Río Corcovado valley. This basin displays a high concentration of glaciolacustrine sediment accumulations on its low-gradient basal surface. The hillshade was replaced with a white background on maps C and H to improve visualisation. See Figure 2 for location.

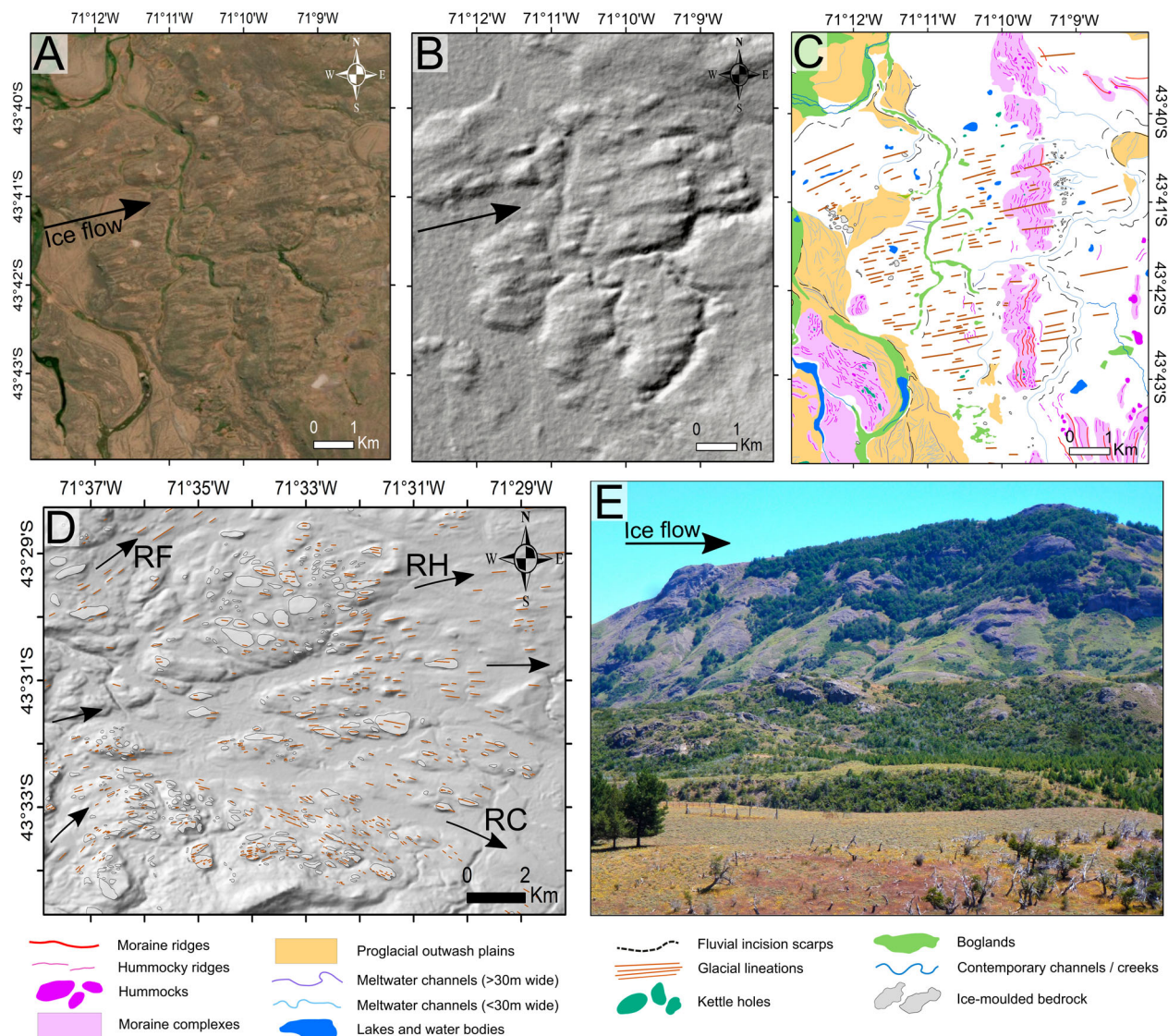


Figure 8. (A) Satellite imagery (ESRITM, DigitalGlobe), (B) DEM hillshade (light azimuth: 315°, incline: 45°) and (C) glacial geomorphological mapping comparisons of the heavily streamlined sediments draped between the eastern Río Corcovado terminal moraine complexes and the Río Huemul valley. These features indicate convergence of the Río Corcovado and Río Huemul outlet glaciers at this location during extensive glaciations. (D) DEM hillshade with glacial lineations and ice-moulded bedrock landforms mapped (with other mapped features removed for visualisation purposes). This bedrock-dominated area presents substantial evidence of subglacial erosion and thus warm-based, fast-flowing ice, and was characterised by the divergence of the PIS into three outlet glaciers: the Río Corcovado glacier to the southeast, the Río Huemul to the east, and the Río Frío (RF) glacier to the northeast. (E) View towards the northwest of ice-moulded bedrock outcrops in the Río Huemul valley (camera location: 43°29'14.16''S, 71°18'23.51''W). See Figure 2 for location.

common in areas of assumed greater former ice-thicknesses, where warm-based, fast-flowing ice could generate either substantial subglacial bedrock erosion, or deposition and/or re-arrangement of glaciogenic sediment along flow lines (Bingham et al., 2017; Clark et al., 2018; Darvill et al., 2014, 2017; Smith et al., 2008). The latter case can lead to the formation of sediment flutes (<10 m in height, Figure 8a–c). Depositional lineations characterised by oval to ellipsoidal shapes and significant positive relief (>10 m) were interpreted and mapped as drumlinoid forms (Knight, 1997; Spagnolo et al., 2012). In the mapped regions, prominent bedrock outcrops ranging from 20 m to 1 km in width often demonstrate large-scale streamlining (Davies et al., 2020; Figure 8d,e). Individual

outcrops displaying such properties were interpreted and mapped as ice-moulded bedrock. The regional distribution and orientation of subglacial lineations including sediment flutes, drumlinoid features and ice-moulded bedrock outcrops are useful indicators of former ice-flow direction (Bentley et al., 2005; Boulton & Clark, 1990). For instance, at our field site, they enable asserting the former convergence of the Río Corcovado and Río Huemul outlets (Figure 8a–c).

5. Summary and conclusions

Our map illustrates the sediment-landform assemblages formed by the Quaternary fluctuations of three outlet glaciers in the northeastern sector of the

former Patagonian Ice Sheet, the Río Corcovado, Río Huemul and Lago Palena/General Vintter outlet glaciers. This map builds on previous local geological (Haller et al., 2003) and broad-scale glacial geomorphological mapping (Caldenius, 1932; Davies et al., 2020; Glasser & Jansson, 2008) to deliver the first detailed glacial geomorphological map of these valley systems. The mapped landforms incorporate well-established glacial geomorphological features of four major depositional and erosional domains: (1) ice-contact glaciogenic landforms (moraine ridges, hummocks, hummocky ridges, kettle holes, moraine complexes and kettle-kame topography) highlighting the former expansion of outlet glaciers into the Argentine foreland; (2) glaciofluvial landforms (proglacial outwash plains, meltwater channels, fluvial incision scarps, potential glacial lake outburst flood deposits) providing detailed geolocation of former meltwater drainage pathways; (3) glaciolacustrine landforms (palaeo-shorelines, raised deltas and glaciolacustrine deposits) indicating the past formation of ice-dammed proglacial lakes following glacier retreat; and (4) subglacial landforms (ice moulded bedrock, glacial lineations and drumlinoid forms) diagnostic of ice-flow direction and glacier basal conditions.

This map will underpin geomorphological and geochronological investigations aimed at reconstructing the former behaviour of the Río Corcovado, Río Huemul and Lago Palena/General Vintter outlet glaciers during Quaternary glacial cycles. It will also represent an essential geographical dataset for investigations aiming to reconstruct former glaciolacustrine systems as well as major shifts in fluvial drainage pathways during and following local glaciations. Finally, this map provides local empirical boundaries that could be used for high-resolution glacial or ice sheet-scale numerical modelling investigations.

Software

Geomorphological mapping through polyline and polygon shapefile digitisation was conducted using ArcGIS 10.6 software. Final map and figure editing was produced using Adobe Illustrator CC 2020 and Inkscape 0.92.4.

Geolocation information

The study area presented within this map is located between these coordinates:

70°44'0"W – 71°40'0"W; 43°24'0"S – 44°2'0"S

Open Scholarship

This article has earned the [Center for Open Science](#) badges for Open Data and Open Materials through Open Practices Disclosure. The data and materials

are openly accessible at 10.17632/c2hy8rkbyd.1 and 10.17632/c2hy8rkbyd.1.

Acknowledgments

We wish to express our most sincere gratitude towards all individuals who contributed to the crowdfunding campaign enabling a 2020 field trip to our study site. We also thank the local landowners who authorised access and work on their property, in particular, the Estancia Tecka (Chubut, Argentina) for enabling access to their land and private roads. Moreover, we are grateful to Juan Luis García, Pablo Tapia Gonzalez, Fabian Riquelme and Martin Toro for help in the field and Chiara Van den Hoven for support with figure production and the use of Adobe Illustrator. We thank Professor Neil F. Glasser for sharing shapefiles aiding initial fieldsite determination. Finally, we wish to thank Professor Jasper Knight, Dr. Jacob M. Bendle, Dr. Harold Lovell and Dr. Heike Apps for their reviews and contributions to improve the manuscript and map.

Disclosure statement

No potential conflict of interest was reported by the authors.

Funding

This investigation is part of a Natural Environment Research Council (NERC) University of Edinburgh E³ Doctoral Training Partnership Ph.D. studentship (award code: NE/L002558/1) awarded to TPML. Our second field expedition (January/February 2020) was supported by a crowd-funding campaign through the Crowd. Science fundraising platform (<https://crowd.science>) and a British Society for Geomorphology Postgraduate Research Grant award (BSG-2019-04) awarded to TPML. Fieldwork in the Lago Palena/General Vintter valley was supported by a Ph.D. Fellowship National Commission of Scientific and Technological Research (#21161417) awarded to RLS and by the ANIS Millennium Science Initiative/millennium Nucleus Paleoclimate (NCN17_079) for EAS, RLS, and MAM.

Map Shapefiles

The data produced for this map are freely available online, as long as original publication is cited when used and/or referred to. This includes twenty-six shapefiles (.shp) necessary for visualising and analysing the data on a geographical information system such as ArcGIS software. The data are deposited in a Mendeley Data online repository, accessible using this DOI:<https://data.mendeley.com/datasets/c2hy8rkbyd/1>.

ORCID

Tancrede P. M. Leger  <http://orcid.org/0000-0001-9098-8312>

Andrew S. Hein  <http://orcid.org/0000-0003-3397-3813>

Robert G. Bingham  <http://orcid.org/0000-0002-0630-2021>

Mateo A. Martini  <http://orcid.org/0000-0003-1704-9313>

Rodrigo L. Soteres  <http://orcid.org/0000-0003-3647-5342>

Esteban A. Sagredo  <http://orcid.org/0000-0002-4494-5423>

References

- Alloway, B. V., Almond, P. C., Moreno, P. I., Sagredo, E., Kaplan, M. R., Kubik, P. W., & Tonkin, P. J. (2018). Mid-latitude trans-Pacific reconstructions and comparisons of coupled glacial/interglacial climate cycles based on soil stratigraphy of cover-beds. *Quaternary Science Reviews*, 189, 57–75. <https://doi.org/10.1016/j.quascirev.2018.04.005>
- Bendle, J. M., Palmer, A. P., Thorndycraft, V. R., & Matthews, I. P. (2017B). High-resolution chronology for deglaciation of the Patagonian Ice Sheet at Lago Buenos Aires (46.5 S) revealed through varve chronology and Bayesian age modelling. *Quaternary Science Reviews*, 177, 314–339. <https://doi.org/10.1016/j.quascirev.2017.10.013>
- Bendle, J. M., Thorndycraft, V. R., & Palmer, A. P. (2017A). The glacial geomorphology of the Lago Buenos Aires and Lago Pueyrredón ice lobes of central Patagonia. *Journal of Maps*, 13(2), 654–673. <https://doi.org/10.1080/17445647.2017.1351908>
- Benn, D. I., & Clapperton, C. M. (2000). Pleistocene glacial-geomorphic landforms and sediments around central Magellan Strait, southernmost Chile: Evidence for fast outlet glaciers with cold-based margins. *Quaternary Science Reviews*, 19(6), 591–612. [https://doi.org/10.1016/S0277-3791\(99\)00012-8](https://doi.org/10.1016/S0277-3791(99)00012-8)
- Benn, D. I., & Evans, D. J. (2014). *Glaciers and glaciation*. Routledge.
- Benn, D. I., Warren, C. R., & Mottram, R. H. (2007). Calving processes and the dynamics of calving glaciers. *Earth-Science Reviews*, 82(3–4), 143–179. <https://doi.org/10.1016/j.earscirev.2007.02.002>
- Bentley, M. J., Sugden, D. E., Hulton, N. R., & McCulloch, R. D. (2005). The landforms and pattern of deglaciation in the Strait of Magellan and Bahía Inútil, southernmost South America. *Geografiska Annaler: Series A, Physical Geography*, 87(2), 313–333. <https://doi.org/10.1111/j.0435-3676.2005.00261.x>
- Bingham, R. G., Vaughan, D. G., King, E. C., Davies, D., Cornford, S. L., Smith, A. M., Arthern, R. J., Brisbourne, A. M., De Rydt, J., Graham, A. G. C., Spagnolo, M., Marsh, O. J., & Shean, D. E. (2017). Diverse landscapes beneath Pine Island Glacier influence ice flow. *Nature Communications*, 8(1), 1–9. <https://doi.org/10.1038/s41467-017-01597-y>
- Blair, T. C. (2002). Alluvial-fan sedimentation from a glacial-outburst flood, Lone Pine, California, and contrasts with meteorological flood deposits. *Flood and Megaflood Processes and Deposits: Recent and Ancient Examples*, 111–140. <https://doi.org/10.1002/9781444304299.ch8>
- Boulton, G. S., & Clark, C. D. (1990). The Laurentide ice sheet through the last glacial cycle: The topology of drift lineations as a key to the dynamic behaviour of former ice sheets. *Transactions of the Royal Society of Edinburgh: Earth Sciences*, 81(4), 327–347. <https://doi.org/10.1017/S0263593300020836>
- Caldenius, C. C. Z. (1932). Las glaciaciones cuaternarias en la patagonia y tierra del fuego. *Geografiska Annaler*, 14, 1–164. <https://doi.org/10.1080/20014422.1932.11880545>
- Chandler, B. M., Lovell, H., Boston, C. M., Lukas, S., Barr, I. D., Benediktsson, Í. Ö., Benn, D. I., Clark, C. D., Darvill, C. M., Evans, D. J., & Ewertowski, M. W. (2018). Glacial geomorphological mapping: A review of approaches and frameworks for best practice. *Earth-Science Reviews*, 185, 806–846. <https://doi.org/10.1016/j.earscirev.2018.07.015>
- Clapperton, C. M. (1993). *Quaternary geology and geomorphology of South America* (Vol. 25). Elsevier.
- Clapperton, C. M., Sugden, D. E., Kaufman, D. S., & McCulloch, R. D. (1995). The last glaciation in central Magellan Strait, southernmost Chile. *Quaternary Research*, 44(2), 133–148. <https://doi.org/10.1006/qres.1995.1058>
- Clark, C. D., Ely, J. C., Greenwood, S. L., Hughes, A. L., Meehan, R., Barr, I. D., Bateman, M. D., Bradwell, T., Doole, J., Evans, D. J., & Jordan, C. J. (2018). BRITICE glacial Map, version 2: A map and GIS database of glacial landforms of the last British–Irish Ice Sheet. *Boreas*, 47(1), 11–e8. <https://doi.org/10.1111/bor.12273>
- Coronato, A., Ercolano, B., Corbella, H., & Tiberi, P. (2013). Glacial, fluvial and volcanic landscape evolution in the Laguna Potrok Aike maar area, Southern Patagonia, Argentina. *Quaternary Science Reviews*, 71, 13–26. <https://doi.org/10.1016/j.quascirev.2012.06.019>
- Darvill, C. M., Bentley, M. J., Stokes, C. R., Hein, A. S., & Rodés, Á. (2015). Extensive MIS 3 glaciation in southernmost Patagonia revealed by cosmogenic nuclide dating of outwash sediments. *Earth and Planetary Science Letters*, 429, 157–169. <https://doi.org/10.1016/j.epsl.2015.07.030>
- Darvill, C. M., Bentley, M. J., Stokes, C. R., & Shulmeister, J. (2016). The timing and cause of glacial advances in the southern mid-latitudes during the last glacial cycle based on a synthesis of exposure ages from Patagonia and New Zealand. *Quaternary Science Reviews*, 129, 200–214. <https://doi.org/10.1016/j.quascirev.2016.07.02410.1016/j.epsl.2015.07.030>
- Darvill, C. M., Stokes, C. R., Bentley, M. J., Evans, D. J., & Lovell, H. (2017). Dynamics of former ice lobes of the southernmost Patagonian Ice Sheet based on a glacial landsystems approach. *Journal of Quaternary Science*, 32(6), 857–876. <https://doi.org/10.1002/jqs.2890>
- Darvill, C. M., Stokes, C. R., Bentley, M. J., & Lovell, H. (2014). A glacial geomorphological map of the southernmost ice lobes of Patagonia: the Bahía Inútil–San Sebastián, Magellan, Otway, Skyring and Río Gallegos lobes. *Journal of Maps*, 10(3), 500–520. <https://doi.org/10.1080/17445647.2014.890134>
- Davies, B. J., Darvill, C. M., Lovell, H., Bendle, J. M., Dowdeswell, J. A., Fabel, D., Garcia, J.-L., Geiger, A., Glasser, N. F., Gheorghiu, D. M., Harrison, S., Hein, A. S., Kaplan, M. R., Martin, J. R. V., Mendelova, M., Palmer, A., Pelto, M., Rodes, A., Sagredo, E. A., ... Thorndycraft, V. R. (2020). The evolution of the Patagonian Ice Sheet from 35 ka to the Present Day (PATICE). *Earth-Science Reviews*, 204, 103152. <https://doi.org/10.1016/j.earscirev.2020.103152>
- Davies, B. J., Thorndycraft, V. R., Fabel, D., & Martin, J. R. V. (2018). Asynchronous glacier dynamics during the Antarctic Cold Reversal in central Patagonia. *Quaternary Science Reviews*, 200, 287–312. <https://doi.org/10.1016/j.quascirev.2018.09.025>
- Denton, G. H., Lowell, T. V., Heusser, C. J., Schlüchter, C., Andersen, B. G., Heusser, L. E., Moreno, P. I., & Marchant, D. R. (1999). Geomorphology, stratigraphy, and radiocarbon chronology of Llanquihue Drift in the area of the Southern Lake District, Seno Reloncaví, and Isla Grande de Chiloé, Chile. *Geografiska Annaler, Series A: Physical Geography*, 81(2), 167–229. <https://doi.org/10.1111/j.0435-3676.1999.00057.x>
- Dunai, T. J. (2010). *Cosmogenic Nuclides: Principles, concepts and applications in the Earth surface sciences*. Cambridge University Press.
- Evans, D. J. A. (2014). *Glacial landsystems*. Routledge.

- Evans, D. J. A., & Orton, C. (2015). Heinabergsjökull and Skalafellsjökull, Iceland: Active temperate piedmont lobe and outwash head glacial landsystem. *Journal of Maps*, 11(3), 415–431. <https://doi.org/10.1080/17445647.2014.919617>
- Eyles, N., Boyce, J. I., & Barendregt, R. W. (1999). Hummocky moraine: Sedimentary record of stagnant Laurentide Ice Sheet lobes resting on soft beds. *Sedimentary Geology*, 123(3–4), 163–174. [https://doi.org/10.1016/S0037-0738\(98\)00129-8](https://doi.org/10.1016/S0037-0738(98)00129-8)
- García, J. L., Hein, A. S., Binnie, S. A., Gómez, G. A., González, M. A., & Dunai, T. J. (2018). The MIS 3 maximum of the Torres del Paine and Última Esperanza ice lobes in Patagonia and the pacing of southern mountain glaciation. *Quaternary Science Reviews*, 185, 9–26. <https://doi.org/10.1016/j.quascirev.2018.01.013>
- García, J. L., Maldonado, A., de Porras, M. E., Delaunay, A. N., Reyes, O., Ebensperger, C. A., Binnie, S. A., Lüthgens, C., & Méndez, C. (2019). Early deglaciation and paleolake history of Río Cisnes glacier, Patagonian ice sheet (44° S). *Quaternary Research*, 91(1), 194–217. <https://doi.org/10.1017/qua.2018.93>
- Garreaud, R., Lopez, P., Minvielle, M., & Rojas, M. (2013). Large-scale control on the Patagonian climate. *Journal of Climate*, 26(1), 215–230. <https://doi.org/10.1175/JCLI-D-12-00001.1>
- Glasser, N., & Jansson, K. (2008). The glacial map of southern South America. *Journal of Maps*, 4(1), 175–196. <https://doi.org/10.4113/jom.2008.1020>
- Glasser, N. F., Jansson, K. N., Duller, G. A., Singarayer, J., Holloway, M., & Harrison, S. (2016). Glacial lake drainage in Patagonia (13–8 kyr) and response of the adjacent Pacific Ocean. *Scientific Reports*, 6(1), 21064. <https://doi.org/10.1038/srep21064>
- Glasser, N. F., Jansson, K. N., Harrison, S., & Kleman, J. (2008). The glacial geomorphology and Pleistocene history of South America between 38°S and 56°S. *Quaternary Science Reviews*, 27(3–4), 365–390. <https://doi.org/10.1016/j.quascirev.2007.11.011>
- Haller, M., Lech, R. R., Martínez, O. A., Meister, C. M., & Page, S. M. (2003). *Hoja Geológica 4373IV/III, Trevelin, Provincia del Chubut. Programa Nacional de Cartas Geológicas de la Republica Argentina, 1:250.000*. Servicio Geológico Nacional.
- Hein, A. S., Coge, A., Darvill, C. M., Mendelova, M., Kaplan, M. R., Herman, F., Dunai, T. J., Norton, K., Xu, S., Christl, M., & Rodés, Á. (2017). Regional mid-Pleistocene glaciation in central Patagonia. *Quaternary Science Reviews*, 164, 77–94. <https://doi.org/10.1016/j.quascirev.2017.03.023>
- Hein, A. S., Dunai, T. J., Hulton, N. R., & Xu, S. (2011). Exposure dating outwash gravels to determine the age of the greatest Patagonian glaciations. *Geology*, 39(2), 103–106. <https://doi.org/10.1130/G31215.1>
- Hein, A. S., Hulton, N. R., Dunai, T. J., Schnabel, C., Kaplan, M. R., Naylor, M., & Xu, S. (2009). Middle Pleistocene glaciation in Patagonia dated by cosmogenic-nuclide measurements on outwash gravels. *Earth and Planetary Science Letters*, 286(1–2), 184–197. <https://doi.org/10.1016/j.epsl.2009.06.026>
- Hein, A. S., Hulton, N. R., Dunai, T. J., Sugden, D. E., Kaplan, M. R., & Xu, S. (2010). The chronology of the Last Glacial Maximum and deglacial events in central Argentine Patagonia. *Quaternary Science Reviews*, 29(9–10), 1212–1227. <https://doi.org/10.1016/j.quascirev.2010.01.020>
- Henríquez, W. I., Villa-Martínez, R., Vilanova, I., Pol-Holz, R. D., & Moreno, P. I. (2017). The Last Glacial Termination on the eastern flank of the central Patagonian Andes (47°S). *Climate of the Past*, 13(7), 879–895. <https://doi.org/10.5194/cp-13-879-2017>
- Hubbard, A., Hein, A. S., Kaplan, M. R., Hulton, N. R., & Glasser, N. (2005). A modelling reconstruction of the last glacial maximum ice sheet and its deglaciation in the vicinity of the Northern Patagonian Icefield, South America. *Geografiska Annaler: Series A, Physical Geography*, 87(2), 375–391. <https://doi.org/10.1111/j.0435-3676.2005.00264.x>
- Iglesias, V., Markgraf, V., & Whitlock, C. (2016). 17,000 years of vegetation, fire and climate change in the eastern foothills of the Andes (lat. 44° S). *Palaeogeography, Palaeoclimatology, Palaeoecology*, 457, 195–208. <https://doi.org/10.1016/j.palaeo.2016.06.008>
- Kaplan, M. R., Hein, A. S., Hubbard, A., & Lax, S. M. (2009). Can glacial erosion limit the extent of glaciation? *Geomorphology*, 103(2), 172–179. <https://doi.org/10.1016/j.geomorph.2008.04.020>
- Knight, J. (1997). Morphological and morphometric analyses of drumlin bedforms in the Omagh Basin, north central Ireland. *Geografiska Annaler: Series A, Physical Geography*, 79(4), 255–266. <https://doi.org/10.1111/j.0435-3676.1997.00021.x>
- Knight, J. (2011). Uses and limitations of field mapping of lowland glaciated landscapes. *Developments in Earth Surface Processes*, 15, 533–550. <https://doi.org/10.1016/B978-0-444-53446-0.00021-5>
- Lambeck, K., Rouby, H., Purcell, A., Sun, Y., & Sambridge, M. (2014). Sea level and global ice volumes from the Last Glacial Maximum to the Holocene. *Proceedings of the National Academy of Sciences*, 111(43), 15296–15303. <https://doi.org/10.1073/pnas.1411762111>
- Lapido, O. (1990). Glacial deposits on the Patagonian Cordillera at latitude 43°30' south. *Quaternary of South America and Antarctic Peninsula*, 6, 257–266.
- Martin, J. R., Davies, B. J., & Thorndycraft, V. R. (2019). Glacier dynamics during a phase of Late Quaternary warming in Patagonia reconstructed from sediment landform associations. *Geomorphology*, 337, 111–133. <https://doi.org/10.1016/j.geomorph.2019.03.007>
- Martínez, O. (2002). *Geomorfología y geología de los depósitos glaciares y periglaciares de la región comprendida entre los 43° y 44° lat. Sur y 70°30' y 72° long. Oeste, Chubut, República Argentina* [Unpublished doctoral thesis]. Universidad Nacional de la Patagonia-San Juan Bosco, Comodoro Rivadavia and Esquel.
- Martínez, O., Coronato, A., & Rabassa, J. (2011). Pleistocene glaciations in northern Patagonia, Argentina: An updated review. *Developments in Quaternary Sciences*, 15, 729–734. <https://doi.org/10.1016/B978-0-444-53447-7.00052-0>
- Mendelová, M., Hein, A. S., McCulloch, R., & Davies, B. (2017). The Last Glacial Maximum and deglaciation in central Patagonia, 44° S–49° S. *Cuadernos de Investigación Geográfica*, 43(2), 719–750. <https://doi.org/10.18172/cig.3263>
- Mendelová, M., Hein, A. S., Rodés, Á., & Xu, S. (2020). Extensive mountain glaciation in central Patagonia during Marine Isotope Stage 5. *Quaternary Science Reviews*, 227, 105996. <https://doi.org/10.1016/j.quascirev.2019.105996>
- Moreiras, S. M., Páez, M. S., Lauro, C., & Jeanneret, P. (2017). First cosmogenic ages for glacial deposits from the Plata range (33°S): New inferences for Quaternary landscape evolution in the Central Andes. *Quaternary International*, 438, 50–64. <https://doi.org/10.1016/j.quaint.2016.08.041>

- Olszak, J. (2011). Evolution of fluvial terraces in response to climate change and tectonic uplift during the Pleistocene: Evidence from Kamienica and Ochotnica River valleys (Polish Outer Carpathians). *Geomorphology*, 129(1–2), 71–78. <https://doi.org/10.1016/j.geomorph.2011.01.014>
- Price, R. J. (1969). Moraines, sandar, kames and eskers near Breidamerkurjökull, Iceland. *Transactions of the Institute of British Geographers*, 17–43. <https://doi.org/10.2307/621406>
- Rabassa, J., Coronato, A., Bujalesky, G., Salemme, M., Roig, C., Meglioli, A., Heusser, C., Gordillo, S., Roig, F., Borronei, A., & Quattrocchio, M. (2000). Quaternary of Tierra del Fuego, southernmost South America: An updated review. *Quaternary International*, 68, 217–240. <https://doi.org/10.5027/andgeoV5n1-a01>
- Raedeke, L. D. (1978). Formas del terreno y depósitos cuaternarios, Tierra del Fuego Central, Chile. *Revista geológica de Chile: An International Journal on Andean Geology*, 5, 3–31. [https://doi.org/10.1016/S1040-6182\(00\)00046-X](https://doi.org/10.1016/S1040-6182(00)00046-X)
- Russell, A. J., Roberts, M. J., Fay, H., Marren, P. M., Cassidy, N. J., Tweed, F. S., & Harris, T. (2006). Icelandic jökulhlaup impacts: Implications for ice-sheet hydrology, sediment transfer and geomorphology. *Geomorphology*, 75(1–2), 33–64. <https://doi.org/10.1016/j.geomorph.2005.05.018>
- Sagredo, E. A., Moreno, P. I., Villa-Martínez, R., Kaplan, M. R., Kubik, P. W., & Stern, C. R. (2011). Fluctuations of the Última Esperanza ice lobe (52°S), Chilean Patagonia, during the last glacial maximum and termination 1. *Geomorphology*, 125(1), 92–108. <https://doi.org/10.1016/j.geomorph.2010.09.007>
- Sissons, J. B. (1978). The parallel roads of Glen Roy and adjacent glens, Scotland. *Boreas*, 7(4), 229–244. <https://doi.org/10.1111/j.1502-3885.1978.tb00281.x>
- Smedley, R. K., Glasser, N. F., & Duller, G. A. T. (2016). Luminescence dating of glacial advances at Lago Buenos Aires (~ 46°S), Patagonia. *Quaternary Science Reviews*, 134, 59–73. <https://doi.org/10.1016/j.quascirev.2015.12.010>
- Smith, M. J., Knight, J., Field, K. S., & Harrison, S. (2008). Glacial striae observations for Ireland compiled from historic records. *Journal of Maps*, 4(1), 378–398. <https://doi.org/10.4113/jom.2008.1035>
- Soteres, R. L., Peltier, C., Kaplan, M. R., & Sagredo, E. A. (2020). Glacial geomorphology of the Strait of Magellan ice lobe, southernmost Patagonia, South America. *Journal of Maps*, 16(2), 299–312. <https://doi.org/10.1080/17445647.2020.1736197>
- Spagnolo, M., Clark, C. D., & Hughes, A. L. (2012). Drumlin relief. *Geomorphology*, 153–154, 179–191. <https://doi.org/10.1016/j.geomorph.2012.02.023>
- Tarolli, P., & Mudd, S. M. (2019). *Remote sensing of geomorphology* (Vol. 23). Elsevier.
- Thorndycraft, V. R., Bendle, J. M., Benito, G., Davies, B. J., Sancho, C., Palmer, A. P., Fabel, D., Medialdea, A., & Martin, J. R. (2019). Glacial lake evolution and Atlantic-Pacific drainage reversals during deglaciation of the Patagonian Ice Sheet. *Quaternary Science Reviews*, 203, 102–127. <https://doi.org/10.1016/j.quascirev.2018.10.036>
- Turner, K. J., Fogwill, C. J., McCulloch, R. D., & Sugden, D. E. (2005). Deglaciation of the eastern flank of the North Patagonian Icefield and associated continental-scale lake diversions. *Geografiska Annaler: Series A, Physical Geography*, 87(2), 363–374. <https://doi.org/10.1111/j.0435-3676.2005.00263.x>
- Van Daele, M., Bertrand, S., Meyer, I., Moernaut, J., Vandoorne, W., Siani, G., Tanghe, N., Ghazoui, Z., Pino, M., Urrutia, R., & De Batist, M. (2016). Late Quaternary evolution of Lago Castor (Chile, 45.6 S): Timing of the deglaciation in northern Patagonia and evolution of the southern westerlies during the last 17 kyr. *Quaternary Science Reviews*, 133, 130–146. [doi:10.1016/j.quascirev.2015.12.021](https://doi.org/10.1016/j.quascirev.2015.12.021)